THE JOURNAL OF PHYSICAL CHEMISTRY C

Article

pubs.acs.org/JPCC

# Disentangling the Effects of Shape and Dielectric Response in van der Waals Interactions between Anisotropic Bodies

Jaime C. Hopkins,[†] Rudolf Podgornik,[*,†,¶,§,⊥] Wai-Yim Ching,[‖] Roger H. French,[⊥,#] and V. Adrian Parsegian[†]

[†]Department of Physics, University of Massachusetts, Amherst, Massachusetts 01003, United States

[¶]Department of Theoretical Physics, Jozef Stefan Institute, SI-1000 Ljubljana, Slovenia

[§]Department of Physics, Faculty of Mathematics and Physics, University of Ljubljana, SI-1000 Ljubljana, Slovenia

[‖]Department of Physics and Astronomy, University of Missouri, Kansas City, Missouri 64110, United States

[⊥]Department of Macromolecular Science and Engineering, Case Western Reserve University, Cleveland, Ohio 44106, United States

[#]Department of Physics, Case Western Reserve University, 10900 Euclid Avenue, Cleveland, Ohio 44106, United States

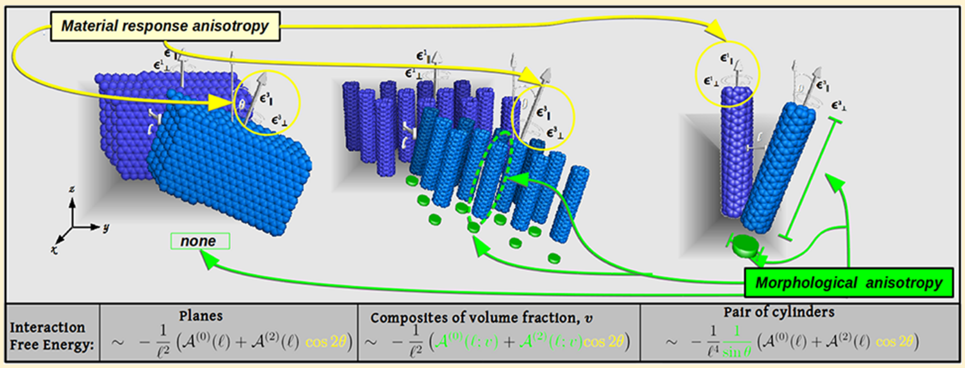


**ABSTRACT:** The free energies, forces, and torques for all separations and mutual orientations are formulated in the full Lifshitz continuum theory of van der Waals interactions. Angular dependence of interactions is characterized for three different interaction geometries of bodies with morphological and/or material anisotropy, interacting across an isotropic aqueous medium: two infinite half-spaces; two half-spaces of composite media comprising parallel cylinder arrays; and an isolated pair of long, thin cylinders. The contributions to van der Waals interaction energy due to shape anisotropy and material anisotropy are isolated in detailed calculations and examined. Surprisingly, the effect of shape on interactions in the retarded regime results in a torque between arrays of cylinders that is stronger than that between half-spaces.

## ■ INTRODUCTION

Effects of anisotropy on van der Waals (vdW) interactions[2] between nanoscale bodies[3] are in general a consequence either of the morphology of the interacting bodies or the electromagnetic response properties of materials of which they are composed.[4] The anisotropy effects in the Lifshitz theory of vdW interactions were first addressed in the inversed configuration, with isotropic boundaries and anisotropic intervening material.[5,6] Later, Parsegian and Weiss[7] independently solved the problem of bodies with anisotropic dielectric response interacting across an isotropic medium in the nonretarded limit. The complete Lifshitz result including retardation was obtained in a veritable *tour de force* by Barash,[8,9] leading to renewed interest in the problem and resulting in a series of developments.[10−13] The general Lifshitz formulas for the interaction between two anisotropic half-spaces or an array of finite-size slabs[14] are algebraically untransparent and involved, probably not permitting any further simplification.[15] Effects of morphological anisotropy have also been studied between anisotropic bodies[16−18] or even between surfaces that have anisotropic decorations.[19,20]

The Barash results for anisotropic dielectrics were then taken as a point of departure in a dilution process[2] for half-spaces composed of long, oriented cylinders, which considers the presence of dielectric cylinders in the dielectric composite as a small perturbation of the dielectric permittivity.[21] This dilution process then results in a pair-interaction free energy between infinitely long cylinders, of isotropic or anisotropic material, at all mutual angles and separations. The first direct attempt to evaluate the interaction between two parallel isotropic cylinders at all separations came from Barash and Kyasov.[22] The interaction for inclined anisotropic cylinders was later obtained from the dilution process, yielding an explicit formula for the angular dependence of the vdW interactions between two

Received: February 25, 2015
Revised: July 23, 2015
Published: July 28, 2015

  

DOI: 10.1021/acs.jpcc.5b01870
J. Phys. Chem. C 2015, 119, 19083−19094

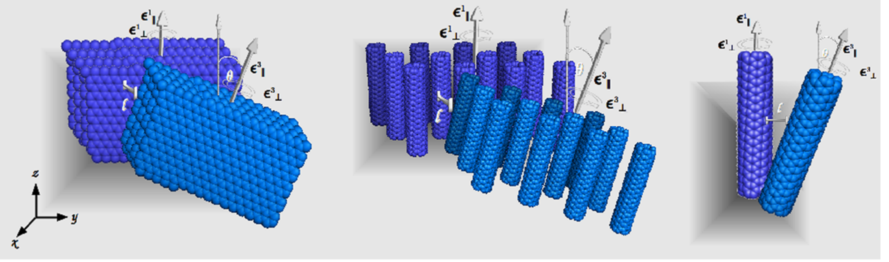

(a) (b) (c)

**Figure 1.** Schematics of the systems of interest with separation $l$ between bodies in isotropic medium and angle, $\theta$, between their principle axes.[1] The isotropic morphology of (a) semi-infinite half-spaces will experience torque only when constructed of anisotropic material. The morphological anisotropy present in (b) composite planes composed of arrays of parallel cylinders and (c) isolated pairs of cylinders will experience torque even when constructed of isotropic material.

infinite cylinders, either with isotropic or anisotropic response, including the nonretarded[23] and retarded limits.[24] These results can be further generalized to cylinders and anisotropic semi-infinite layers,[25,26] a direction we will not pursue here. Orientation dependence of the Casimir, i.e., zero temperature, interaction for perfect metallic cylinders, either parallel[27] or inclined,[28] over a wide range of separations was also studied via the scattering approach[29] for nonplanar objects at zero temperature and in the classical high-temperature limit.

An unequivocal conclusion of the studies of anisotropies on vdW interactions is that their angular dependence shows up in two different ways, corresponding to shape anisotropy and the material anisotropy. The effect is fundamentally nonadditive: anisotropic shapes with isotropic material response as well as isotropic shapes with anisotropic material response can both show equally strong anisotropy effects in the vdW interactions, i.e., forces and torques. Therefore, what thus remains to be analyzed is what part of the general angular dependence of the vdW interaction between anisotropic bodies is due to the shape anisotropy, what part to the material anisotropy, and how to properly disentangle the two closely connected effects.

To answer these queries, we will investigate the vdW interactions in the full Lifshitz theory for several separate cases schematically represented in Figure 1: two homogeneous semi-infinite planar dielectric bodies with anisotropic dielectric response, two inhomogeneous semi-infinite dielectric composites with embedded arrays either of isotropic or anisotropic cylinders, two interacting cylinders composed of isotropic materials, and finally two interacting cylinders composed of anisotropic material. We will investigate the origin and strength of anisotropy effects in vdW interactions for all the stated cases and identify the regime and/or configurations in which they are the largest. This will allow us to suggest some specific experimental configurations that could exploit these newly identified features of vdW interactions between shape and/or material anisotropic bodies.

## ■ THEORETICAL METHODS

**Interaction between Two Semi-Infinite Planar Anisotropic Dielectric Materials.** The complete solution for the problem of vdW interaction between two semi-infinite planar anisotropic dielectric materials interacting across a dielectrically isotropic medium containing no free ions was obtained first by Barash.[8,9] His result reduces to the nonretarded form of Parsegian and Weiss[7] for small separations (1−10 nm) as well as having a fully retarded form for large separations (10−100 nm). The formulas are formidable, mostly because, in contrast to the isotropic case with polarization degeneracy, the surface waves are a particular linear combination of the polarized ordinary and extraordinary waves, leading to a much more complicated algebra that eventually led to a typographical error in the original formulation. The error was then persistently dragged through the literature until finally rectified in erratum.[13] For this reason, the relevant formulas are fully reproduced in Appendix A.

The Barash derivation leads to the vdW interaction free energy for two uniaxial dielectric half spaces as a function of the separation, $l$; the angle between the principal directions of the two uniaxial dielectric tensors, $\theta$; and the dielectric responses of all the media involved: that of the isotropic intervening medium, $\epsilon_m$, as well as the perpendicular, $\epsilon_\perp$, and the parallel, $\epsilon_\parallel$, dielectric responses of the uniaxial semi-infinite media. Their dielectric tensors thus have the form:

$$\epsilon_{ij}^{(1)} = \begin{bmatrix} \epsilon_{1\parallel} & 0 & 0 \\ 0 & \epsilon_{1\perp} & 0 \\ 0 & 0 & \epsilon_{1\perp} \end{bmatrix} \quad \text{and}$$

$$\epsilon_{ij}^{(2)} = \begin{bmatrix} \epsilon_{2\parallel}\cos^2\theta + \epsilon_{2\perp}\sin^2\theta & (\epsilon_{2\perp} - \epsilon_{2\parallel})\sin\theta\cos\theta & 0 \\ (\epsilon_{2\perp} - \epsilon_{2\parallel})\sin\theta\cos\theta & \epsilon_{2\parallel}\sin^2\theta + \epsilon_{2\perp}\cos^2\theta & 0 \\ 0 & 0 & \epsilon_{2\perp} \end{bmatrix} \tag{1}$$

The frequency-dependent dielectric responses involved in eq 1 in general imply also optical birefringence. The free energy of vdW interaction per unit area for two uniaxial anisotropic half spaces interacting across an isotropic medium is then obtained in terms of the Hamaker coefficient, $\mathcal{H}(l, \theta)$, (see Appendix A):

$$\mathcal{G}(l, \theta) = -\frac{\mathcal{H}(l, \theta)}{12\pi l^2} \tag{2}$$

where the Hamaker coefficient depends on separation of the bodies and the mutual orientation of the principal directions of the dielectric tensors. It can be evaluated exactly for any value of the separation as well as any anisotropy from formulas eqs 23−31 listed in Appendix A. However, a simple analytic dependence on angle can be obtained in the limit of weak anisotropic inhomogeneity, i.e., in the limit

$$\epsilon_\perp = \epsilon_m(1 + \delta_\perp) \quad \text{and} \quad \epsilon_\parallel = \epsilon_m(1 + \delta_\parallel) \tag{3}$$


DOI: 10.1021/acs.jpcc.5b01870
J. Phys. Chem. C 2015, 119, 19083−19094

for small but otherwise arbitrary $\delta_\perp, \delta_\parallel \ll 1$. One can derive the interaction free energy in the explicit form to the second order in $\delta_\perp, \delta_\parallel$ as

$$\mathcal{G}(l, \theta) = \frac{k_B T}{2\pi} \sum_{n=0}^{\infty}{}' \int_0^\infty Q \, dQ \, f(Q, \omega_n; l, \theta) + O(\delta_\perp^3, \delta_\parallel^3) \quad (4)$$

with

$$f(Q, \omega_n; l, \theta) = \frac{1}{128} \frac{\exp\left(-2l\sqrt{Q^2 + \epsilon_m \frac{\omega_n^2}{c^2}}\right)}{(Q^2 + \epsilon_m \frac{\omega_n^2}{c^2})^2} \left\{ 2\left[ (\delta_\parallel + 3\delta_\perp)^2 Q^4 + 2(\delta_\parallel + 3\delta_\perp)(\delta_\parallel + \delta_\perp) Q^2 \epsilon_m \frac{\omega_n^2}{c^2} + 2(\delta_\parallel + \delta_\perp)^2 \epsilon_m^2 \frac{\omega_n^4}{c^4} \right] + (\delta_\parallel - \delta_\perp)^2 \left( Q^2 + 2\epsilon_m \frac{\omega_n^2}{c^2} \right)^2 \cos 2\theta \right\} \quad (5)$$

The angular dependence of $\mathcal{G}(l, \theta)$, and consequently of $\mathcal{H}(l, \theta)$, in this limit obviously assumes a particularly simple, explicit analytical form. In the general case, the full Barash formulas do not yield a simply extractable analytic angular dependence, but numeric results can always be represented with

$$\mathcal{H}(l, \theta) = \mathcal{A}^{(0)}(l) + \mathcal{A}^{(2)}(l) \cos(2\theta) \quad (6)$$

where the separation-dependent isotropic and anisotropic parts of the Hamaker coefficient, $\mathcal{A}^{(0)}(l)$ and $\mathcal{A}^{(2)}(l)$, respectively, allow for a straightforward analysis of the angular dependence of the free energy. $\mathcal{A}^{(0)}$ is obtained by choosing the value of $\theta$ such that the angular contributions to the Hamaker coefficient, $\mathcal{H}(l, \theta)$ become zero, i.e., $\mathcal{H}(l, \theta = \pi/4) = \mathcal{A}^{(0)}(l)$. Subsequently, $\mathcal{A}^{(2)}(l)$ is obtained from the resulting difference in $\mathcal{H}(l, \theta) - \mathcal{A}^{(0)}(l)$.

The force per unit area, $g(l, \theta)$, and the torque per unit area, $\tau(l, \theta)$, can be obtained straightforwardly as

$$g(l, \theta) = -\frac{\partial \mathcal{G}(l, \theta)}{\partial l} \quad \text{and}$$
$$\tau(l, \theta) = -\frac{\partial \mathcal{G}(l, \theta)}{\partial \theta} = -\frac{\mathcal{A}^{(2)}(l) \sin(2\theta)}{6\pi l^2} \quad (7)$$

The force per unit area has a complicated dependence on $l$ because of the explicit $l^{-2}$-dependence of the free energy and the $l$-dependences of $\mathcal{A}^{(0)}(l)$ and $\mathcal{A}^{(2)}(l)$. While the $l$-dependence of $g(l, \theta)$ is complicated, the angular dependence of the torque per unit area can be written as a simple $\sin(2\theta)$ dependence with an $l$-dependent prefactor.

The vdW interaction between semi-infinite planes that are made of isotropic dielectric materials, i.e., $\epsilon_\perp = \epsilon_\parallel$, shows no angular dependence, and consequently these isotropic bodies experience no torque. However, this is strictly true only for semi-infinite bodies. Should the two slabs have finite dimensions, the shape anisotropy (see below) would lead to a torque even for isotropic materials.

**Interaction between Two Semi-Infinite Composites Made of Oriented Cylinders.** Planes of composite media are constructed from arrays of parallel cylinders of a given volume fraction embedded in an isotropic medium, with the two arrays inclined with respect to one another. While this configuration has been implicated in (nonretarded) vdW torques before,[30] the relation between the packing density and the strength of vdW torques has not been explicitly considered. The arrays interact as a function of their mutual orientation and separation across a gap of isotropic medium. Formulation of the vdW interaction free energy for composite media follows that of anisotropic half-spaces but with the modification that the media's dielectric response functions reflect the composition of the dielectrically inhomogeneous array.

We now assume that both semi-infinite half-spaces are composite materials made of oriented anisotropic cylinders at the volume fraction $\nu$, with $\epsilon_\perp^c$ and $\epsilon_\parallel^c$ as the transverse and longitudinal dielectric response functions of the cylinder material, respectively. For the semi-infinite composite medium of oriented anisotropic cylinders with local hexagonal packing symmetry, the volume fraction is

$$\nu = \frac{2\pi}{\sqrt{3}} \frac{1}{\left(2 + \frac{\beta}{\alpha}\right)^2} \quad (8)$$

where $\alpha$ is the radius of the cylinder and $\beta$ is the intersurface separation between cylinders. For hexagonal close packing, $\nu$ = 0.91. The anisotropic bulk dielectric response as a function of the imaginary Matsubara frequencies can then be derived in the form[2]

$$\overline{\epsilon}_\perp(i\omega_n, \nu) = \epsilon_m(i\omega_n)\left(1 + \frac{2\nu\Delta_\perp(i\omega_n)}{1 - \nu\Delta_\perp(i\omega_n)}\right) \quad \text{and}$$
$$\overline{\epsilon}_\parallel(i\omega_n, \nu) = \epsilon_m(i\omega_n)(1 + \nu\Delta_\parallel(i\omega_n)) \quad (9)$$

where the relative anisotropy measures in the perpendicular and parallel direction are given by

$$\Delta_\perp(i\omega_n) = \frac{\epsilon_\perp^c(i\omega_n) - \epsilon_m(i\omega_n)}{\epsilon_\perp^c(i\omega_n) + \epsilon_m(i\omega_n)} \quad \text{and}$$
$$\Delta_\parallel(i\omega_n) = \frac{\epsilon_\parallel^c(i\omega_n) - \epsilon_m(i\omega_n)}{\epsilon_m(i\omega_n)} \quad (10)$$

$\epsilon_m$ is assumed to be the dielectric function of the isotropic medium between the cylinders as well as between both semi-infinite regions.

The above formula for cylindrical inclusions is due to Rayleigh and is exact to fifth order in volume fraction for any composite. However, higher-order terms depend on the exact symmetry of the cylinder packing in the array.[31] While other mixing formulations for the composite dielectric function are possible and have been explored in the context of vdW interactions,[32,33] they differ mostly in the higher-order volume fraction terms. Because the problem of the dielectric response of the composite does not possess a general, universally valid solution, approximations are necessary and should be checked for consistency whenever possible. The Rayleigh form possesses the virtue of yielding the correct vdW interaction between a pair of cylinders in the process of dilution[23,24] as described in the next section. Also, in the Rayleigh approach the scattering effects are not taken into account on the level of the dielectric function, which is a drawback of the method, but it does allow


DOI: 10.1021/acs.jpcc.5b01870
J. Phys. Chem. C 2015, 119, 19083−19094

for an exact inclusion of the packing symmetry which would be difficult in other approaches. Rayleigh and Maxwell–Garner mixing rules in fact coincide for up to 15% volume fraction[34] and do not differ fundamentally even for much higher packing fractions.

The vdW interaction free energy, the force, and the torque per unit area then follow from the same formulas as in the previous section, but taking due notice that now the parallel and the perpendicular dielectric responses of the semi-infinite media are given by the dielectric composite relation

$$\epsilon_\perp \to \overline{\epsilon_\perp}(v) \quad \text{and} \quad \epsilon_\parallel \to \overline{\epsilon_\parallel}(v) \tag{11}$$

To lowest order, the Hamaker coefficient is quadratic in $v$, as can be seen by expanding the Barash result, eq 2, and has the explicit form

$$\mathcal{G}(l, \theta) = -v^2 \frac{k_B T}{2\pi} \sum_{n=0}^{\infty}{}' \int_0^\infty Q\, dQ\, f(Q, \omega_n; l, \theta) + O(v^4) \tag{12}$$

where

$$f(Q, \omega_n; l, \theta) = f^{(0)}(Q, \omega_n; l) + f^{(2)}(Q, \omega_n; l) \cos 2\theta \tag{13}$$

with

$$f^{(0)}(Q, \omega_n; l) = \frac{\Delta_\parallel^2}{128} \frac{\exp\left(-2l\sqrt{Q^2 + \epsilon_m \frac{\omega_n^2}{c^2}}\right)}{(Q^2 + \epsilon_m \frac{\omega_n^2}{c^2})^2} \left\{2\left[(1 + 3a)^2 Q^4 + 2(1 + 3a)(1 + a) Q^2 \epsilon_m \frac{\omega_n^2}{c^2}\right]\right\} \tag{14}$$

and

$$f^{(2)}(Q, \omega_n; l) = \frac{\Delta_\parallel^2}{128} \frac{\exp\left(-2l\sqrt{Q^2 + \epsilon_m \frac{\omega_n^2}{c^2}}\right)}{(Q^2 + \epsilon_m \frac{\omega_n^2}{c^2})^2} \left\{(1 - a)^2 \left(Q^2 + 2\epsilon_m \frac{\omega_n^2}{c^2}\right)^2\right\} \tag{15}$$

The ratio of the relative anisotropy measures is defined as

$$a = \frac{2\Delta_\perp}{\Delta_\parallel} = 2\frac{(\epsilon_\perp^c - \epsilon_m)\epsilon_m}{(\epsilon_\perp^c + \epsilon_m)(\epsilon_\parallel^c - \epsilon_m)} \tag{16}$$

The Hamaker coefficient therefore also acquires an additional dependence on the volume fraction of the interacting composites, quadratic to the lowest order, with the general form

$$\mathcal{H}(l, \theta; v) = \mathcal{A}^{(0)}(l; v) + \mathcal{A}^{(2)}(l; v) \cos(2\theta) \tag{17}$$

Unlike the case of vdW interaction between isotropic planes, in the case of dielectric composites made of isotropic cylinders, i.e., $\epsilon_\perp^c = \epsilon_\parallel^c$, we see persistence of angular dependence stemming from the anisotropic *shape* of the cylinders, which is present in all configurations of this type of composite media. The origin of dielectric anisotropy can therefore be traced to either material anisotropy of the interacting homogeneous dielectric materials or to the shapes of the constituent units in the case of dielectric composites.

The force per unit area, $g(l, \theta)$, and the torque per unit area, of $\tau(l, \theta)$, now follow from the same formulas as in the case of two homogeneous anisotropic semi-infinite regions. Again, the force per unit area has a complicated dependence on $l$; the angular dependence of the torque per unit area is simply $\sin(2\theta)$ with an $l$-dependent prefactor.

**Interaction between Two Cylinders Made of (An)-Isotropic Dielectric Materials.** Starting from the interaction free energy of composite media made of arrays of parallel cylinders embedded in an isotropic medium, the interaction free energy of an isolated pair of cylinders is derived by a dilution process, taking the volume fraction of the composite in the dilute limit and expanding the anisotropic dielectric responses to second order in the number density. The coefficient of this term is proportional to the pair-interaction free energy.[2]

To perform this process, we assume that the two anisotropic half-spaces are composed of identical anisotropic cylinders of radii $R_{1,2} = \alpha$, at volume fraction $v$, with $\epsilon_\perp^c$ and $\epsilon_\parallel^c$ as the transverse and longitudinal dielectric response functions of the cylinder materials, respectively. We then expand the Barash interaction free energy $G(l, \theta)$ for two half-spaces again as a series in $v$, eq 12, and evaluate the coefficient multiplying the $v^2$ term. The volume fraction, $v$, scales with the area density of the cylinders ($N$) in the direction of their long axes as $v = N\pi\alpha^2$. It then follows[2] that the interaction free energy between two cylinders, $G(l, \theta)$ , whose axes coincide with the anisotropy axes of the two composites at a separation $l$, inclined at an angle $\theta$, can be obtained from a second derivative of $\mathcal{G}(l, \theta)$ (see Appendix B) as

$$\begin{aligned} N^2 \sin\theta\, G(l, \theta) &= \frac{d^2\mathcal{G}(l, \theta)}{dl^2} \\ &= v^2 \frac{k_B T}{2\pi} \sum_{n=0}^{\infty}{}' \int_0^\infty Q\, dQ \frac{d^2 f(Q, \omega_n; l, \theta)}{dl^2} \end{aligned} \tag{18}$$

where $f(Q, \omega_n; l,\theta)$ is written explicitly in eq 13. Note that such an expansion is possible only if the dielectric response at all frequencies is bounded. In the case of an ideal metal Drude-like dielectric response, this expansion is not feasible and our method cannot be transplanted to that case automatically. By noting that

$$f(Q, \omega_n; l, \theta) = f^{(0)}(Q, \omega_n; l) + f^{(2)}(Q, \omega_n; l) \cos 2\theta \tag{19}$$

$\mathcal{G}(l, \theta)$ can be finally obtained explicitly and exactly as[24]

$$\begin{aligned} \mathcal{G}(l, \theta) &= -\frac{(\pi\alpha^2)^2}{2\pi l^4 \sin\theta} \mathcal{H}(l, \theta) \\ &= -\frac{(\pi\alpha^2)^2}{2\pi l^4 \sin\theta} (\mathcal{A}^{(0)}(l) + \mathcal{A}^{(2)}(l) \cos 2\theta) \end{aligned} \tag{20}$$

where the isotropic and the anisotropic parts of the Hamaker coefficient, i.e. $\mathcal{A}^{(0)}(l)$ and $\mathcal{A}^{(2)}(l)$, can be obtained in explicit forms (given in Appendix B), and they depend on the relative anisotropy measures in the parallel and perpendicular directions, eq 10, at imaginary Matsubara frequencies. The ratio of the relative anisotropy measures, eq 16, can be thought of as a specific measure of the anisotropy of the cylinders



DOI: 10.1021/acs.jpcc.5b01870
J. Phys. Chem. C 2015, 119, 19083−19094

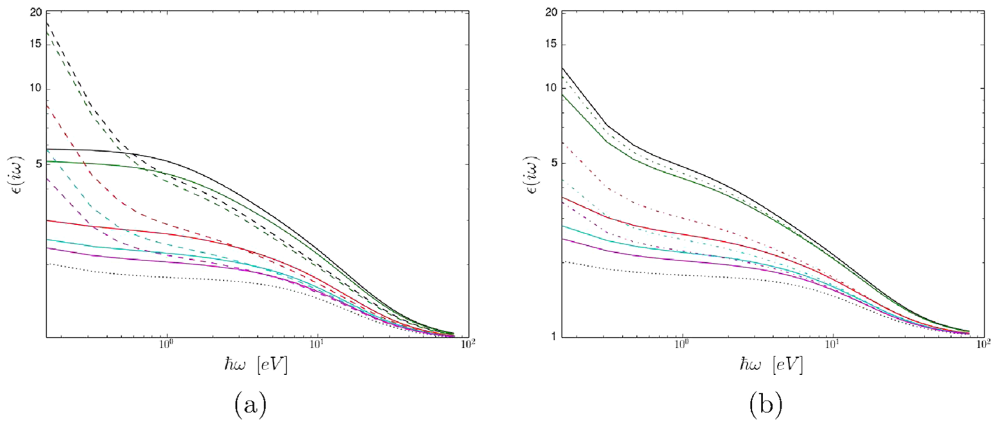


**Figure 2.** Frequency-dependent dielectric response $\epsilon(i\omega)$, with frequency in electronvoltss. (a) The anisotropic bulk dielectric responses, $\epsilon_{\|}$ and $\epsilon_{\perp}$, for semi-infinite planes are shown for [9,3,m] CNTs as black dashed and black solid lines, respectively. The responses for composite media with varied volume fractions of cylindrical inclusions are shown for volume fractions of 0.91 (green), 0.40 (red), 0.23 (cyan), and 0.15 (magenta), corresponding to cylinder separations of 0, $\alpha$, $2\alpha$, and $3\alpha$, respectively, with $\alpha$ = 0.42 nm as the radius of [9,3,m] CNTs. (b) Isotropic bulk dielectric responses are computed from the isometric average of the anisotropic dielectric responses shown in panel a. Though the dielectric responses of the cylindrical inclusions are isotropic (black), the composite dielectric responses become anisotropic because of the anisotropic shape of the cylindrical inclusions.

compared with the isotropic bathing medium, $m$. Note that the relative anisotropy measures vanish when the transverse/longitudinal dielectric response of the cylinder material equals the medium response.

Note also that because of the $\sin^{-1}\theta$ in the free energy, the angular dependence is now associated with both Hamaker coefficients, $\mathcal{A}^{(0)}$ and $\mathcal{A}^{(2)}$, unlike in the case of the semi-infinite planar and composite bodies which have angular dependence associated only with the orientation term, i.e., $\mathcal{A}^{(2)}\cos 2\theta$. Furthermore, the interaction free energy diverges for two parallel cylinders because for two *infinite parallel cylinders* their interaction free energy scales as their length, so that the interaction free energy per unit length remains perfectly finite. We will not be specifically dealing with this anomalous situation as perfect alignment is difficult to envision for any realistic nano-objects.

For cylinders, the force, $\tilde{g}(l, \theta)$, and the torque, $\tilde{\tau}(l, \theta)$, can now be obtained straightforwardly as

$$\tilde{g}(l, \theta) = -\frac{\partial \mathcal{G}(l, \theta)}{\partial l} \tag{21}$$

and

$$\begin{aligned}\tilde{\tau}(l, \theta) &= -\frac{\partial \mathcal{G}(l, \theta)}{\partial \theta} \\ &= -\frac{(\pi\alpha^2)^2}{2\pi l^4}(\mathcal{A}^{(0)} + \mathcal{A}^{(2)}(2 - \cos 2\theta))\frac{\cos\theta}{\sin^2\theta}\end{aligned} \tag{22}$$

The force per unit area has a complicated dependence on $l$, stemming from the explicit $l^{-4}$ dependence of the free energy, as well as both $\mathcal{A}^{(0)}(l)$ and $\mathcal{A}^{(2)}(l)$ that also separately depend on $l$. The angular dependence of the torque can be obtained explicitly and has a complicated angular dependence, partly due to the overall $\sin^{-1}\theta$ dependence of the interaction free energy and partly from the angular dependence of the Hamaker coefficient.

## RESULTS AND DISCUSSION

**Bulk Dielectric Response Function.** In what follows, we specifically consider the dielectric responses of materials that are accessible and relevant to mesoscale interactions in aqueous solutions.[4] As the intervening isotropic solvent, we have taken water with a well-known frequency-dependent dielectric response function[2] as provided by the *Gecko Hamaker* software platform, which also contains an extensive spectral database of various relevant materials.[35] We used the ab initio orthogonalized linear combination of atomic orbital (OLCAO) method[36] to calculate the electronic structures and optical properties of [6,5,s] and [9,3,m] carbon nanotube (CNT) materials.[37] The CNTs represent good examples of materials with highly anisotropic optical properties, and we have used them to characterize the bulk dielectric response of two semi-infinite materials. Other choices are also possible.[4]

The semi-infinite anisotropic composite materials are constructed as arrays of [6,5,s] and [9,3,m] *anisotropic* CNT cylinders embedded in water at various volume fractions, given by eq 8 in terms of the interaxial separation between the cylindrical inclusions in the composite, see Figure 2a. We next constructed anisotropic semi-infinite composites out of *isotropic* cylindrical inclusions. Clearly, here the anisotropic material component is missing and the bulk anisotropy is due to only the morphological anisotropy of the inclusions, see Figure 2b. The isotropic dielectric response of the cylindrical inclusions is computed from the isometric *average* of the perpendicular and parallel responses of the unmodified [6,5,s] and [9,3,m] CNT dielectric spectra. The anisotropic dielectric responses used as inputs for formulas for interacting solid planes or a pair of cylinders are independent of volume fraction, $\epsilon_{\|}$ (dashed black line) and $\epsilon_{\perp}$ (solid black line), are shown for [9,3,m] CNT in Figure 2a. Calculations for interactions between planes or cylinder pairs with isotropic (I) dielectric responses use $\epsilon_{\|}^{\mathrm{I}} = \epsilon_{\perp}^{\mathrm{I}} = (\epsilon_{\|} + \epsilon_{\perp})/2$, shown as a black solid line in Figure 2b.

For planes of composite media composed of cylinders embedded in water, the dielectric responses become dependent on the volume fraction of cylinders, see eq 8. Volume fractions are calculated for separations, $\beta$, between cylinders given as multiples of the cylinder radius, e.g., $\alpha$ = 0.42 nm for [9,3,m]


DOI: 10.1021/acs.jpcc.5b01870
J. Phys. Chem. C 2015, 119, 19083−19094

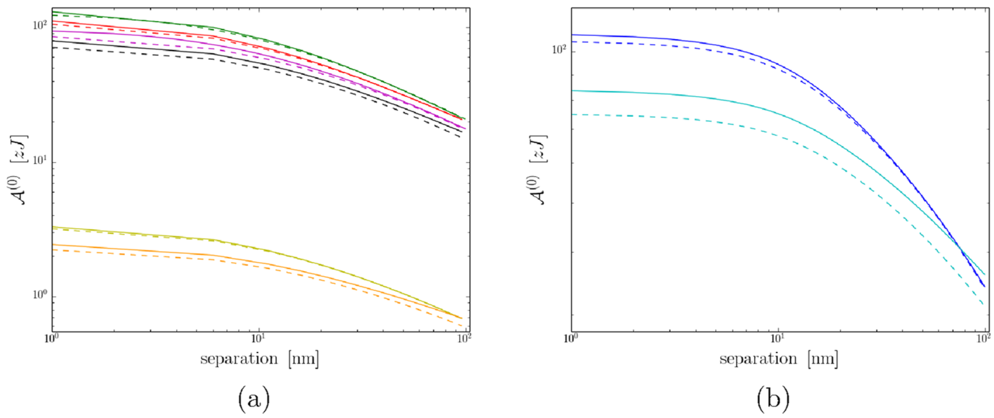


**Figure 3.** (a) The $\mathcal{A}^{(0)}$ term of the Hamaker coefficient for planes ([6,5,s] green, [9,3,m] magenta), and composites of volume fractions 0.91 ([6,5,s] red, [9,3,m] black) and 0.15 ([6,5,s] yellow, [9,3,m] orange) of anisotropic (solid lines) or isotropic material (dashed lines) with a mutual angle, $\theta = \pi/4$, plotted as a function of separation. (b) $\mathcal{A}^{(0)}$ as a function of separation between an isolated pair of long, thin cylinders made either of anisotropic or isotropic [6,5,s] (blue) or [9,3,m] (cyan) CNT material.

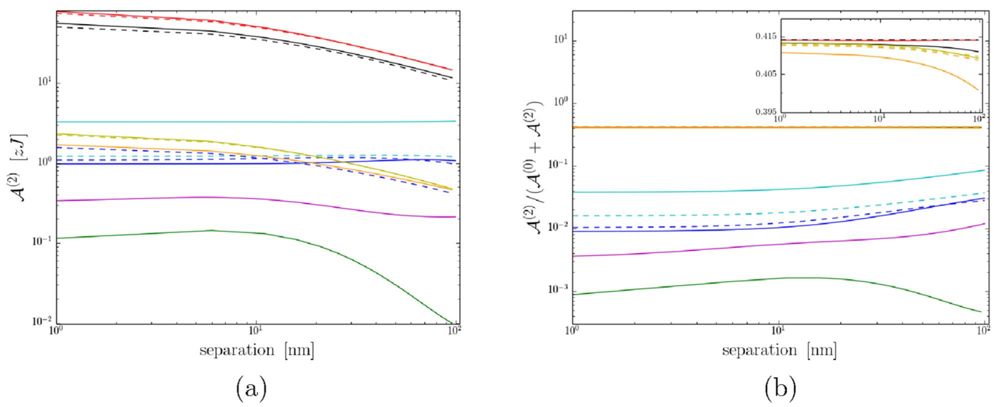


**Figure 4.** (a) $\mathcal{A}^{(2)}$ for an isolated pair of cylinders ([6,5,s] blue, [9,3,m] cyan), planes ([6,5,s] green, [9,3,m] magenta), and composites of volume fractions 0.91 ([6,5,s] red, [9,3,m] black) and 0.15 ([6,5,s] yellow, [9,3,m] orange) of anisotropic (solid lines) or isotropic material (dashed lines) with a mutual angle, $\theta = \pi/4$, plotted as a function of separation. (b) The ratio of $\mathcal{A}^{(2)}$ relative to the total Hamaker coefficient is greatly increased by the morphologically anisotropic cylinders in the composite and pair cylinder cases when compared to the planar cases which contain no morphological anisotropy. The isotropic cases (dashed lines) for composite planes retain their angular dependence because of the shape of the cylindrical inclusions (inset).

CNTs. The parallel responses (dashed lines) and perpendicular responses (solid lines) are plotted in Figure 2a for four volume fractions corresponding to cylinder separations of 0, $\alpha$, $2\alpha$, and $3\alpha$. For composite bodies made of cylinders of isotropic material, $\epsilon_{\parallel}^{\mathrm{I}} = \epsilon_{\perp}^{\mathrm{I}}$ are used as input for eqs 9, leading to anisotropic responses, $\overline{\epsilon}_{\parallel} \neq \overline{\epsilon}_{\perp}$, for the composite body. For decreasing volume fractions of cylinders, the magnitude of anisotropy between $\overline{\epsilon}_{\parallel}$ and $\overline{\epsilon}_{\perp}$, shown as dashed lines and solid lines, respectively, in Figure 2b, decreases as $\overline{\epsilon}_{\parallel}$ and $\overline{\epsilon}_{\perp}$ tend toward the isotropic background response, $\epsilon_{\mathrm{water}}$, dotted line.

**Hamaker Coefficient.** *Effects on $\mathcal{A}^{(0)}$ Term.* We now proceed to the evaluation of the Hamaker coefficients as defined above. We present three different interaction geometries with anisotropic and isotropic materials: planar anisotropic half spaces, planar composite half spaces, and two isolated cylinders.

The orientation-independent coefficient, $\mathcal{A}^{(0)}$, for materials like [6,5,s] and [9,3,m] CNTs shown in Figure 3, is the dominating contributor to the total Hamaker coefficient, $\mathcal{H}$, and consequently, the free energy per unit area for planar and composite bodies, eqs 6 and 17, and the free energy per isolated pair of cylinders, eq 20. For example, at 6 nm separations, $\mathcal{A}^{(0)}$ constitutes approximately 96–99.9% of the total Hamaker coefficient for interacting planes and for an interacting cylinder pair. For interacting composite bodies separated by a 6 nm gap, $\mathcal{A}^{(0)}$ constitutes about 59% of $\mathcal{H}$. For large values of separation, retardation effects are clearly visible and result in smaller values of the Hamaker coefficient.

For interacting planes made of anisotropic [6,5,s] and [9,3,m] CNT materials, shown as solid lines in Figure 3a, we see large values of $\mathcal{A}^{(0)}$ due to the large dielectric contrast at the interface of the bodies and the intervening water medium. For interacting planes made of isotropic material, given by averaging the parallel and perpendicular dielectric responses, the values of $\mathcal{A}^{(0)}$, shown as dashed lines, are less than those of the anisotropic case because of a slightly lower dielectric contrast at the interfaces.

For composite bodies with embedded cylinders made either of anisotropic or isotropic dielectric material, dielectric contrast is reduced at the interface between the bodies and the water

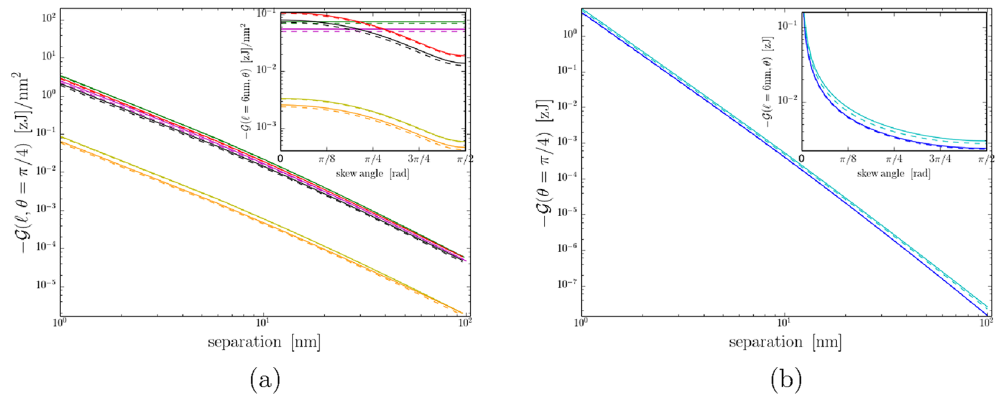


**Figure 5.** (a) Free energy per unit area, $\mathcal{G}$, between planes ([6,5,s] green, [9,3,m] magenta) and composites of volume fractions 0.91 ([6,5,s] red, [9,3,m] black) and 0.15 ([6,5,s] yellow, [9,3,m] orange) of anisotropic (solid lines) or isotropic material (dashed lines) with a mutual angle, $\theta = \pi/4$, plotted as a function of separation. The free energy between composite bodies with a separation of 6 nm as a function of mutual angle (inset) shows an angular-dependence that is dissimilar to that of planes. (b) Free energy per isolated pair of cylinders, $\mathcal{G}$, at a mutual angle of $\theta = \pi/4$, is plotted as a function of separation for cylinders of anisotropic or isotropic [6,5,s] (blue) or [9,3,m] (cyan) material. The cylinder pair shows (inset) an angular dependence stronger than that of planes and composites.

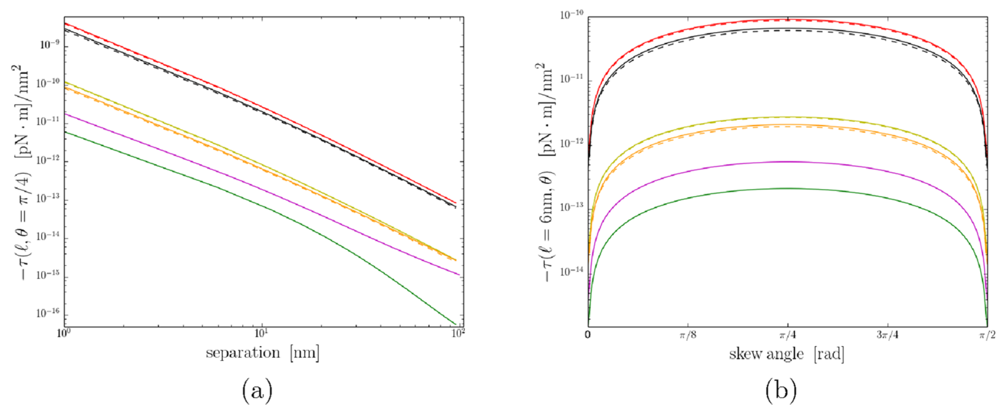


**Figure 6.** (a) Torque per unit surface area, $\tau$, between planes ([6,5,s] green, [9,3,m] magenta) and composites of volume fractions 0.91 ([6,5,s] red, [9,3,m] black) and 0.15 ([6,5,s] yellow, [9,3,m] orange) of anisotropic (solid lines) or isotropic material (dashed lines) with a mutual angle of $\theta = \pi/4$ plotted as a function of separation ($\tau = 0$ for plans of isotropic material). (b) Torque between planes and composite bodies with a separation of 6 nm as a function of mutual angle. Composite bodies experience magnitudes of torque greater than those between planar bodies even when the composite's inclusions are constructed of isotropic material.

gap due to eqs 9 and 11. Thus, the values of $\mathcal{A}^{(0)}$ are reduced compared to the case of interacting planar bodies, see Figure 3a.

For an interacting pair of cylinders, we see $\mathcal{A}^{(0)}$ values that are similar to those for planar and composite cases, see Figure 3. The $\mathcal{A}^{(0)}$ term becomes related to orientation when multiplied by the factor $\sin^{-1}\theta$ in the expression for free energy for a cylinder pair, eq 20.

*Effects on $\mathcal{A}^{(2)}$ Term.* Unlike $\mathcal{A}^{(0)}$, the Hamaker coefficient $\mathcal{A}^{(2)}$ intrinsically carries dependence on the mutual orientation of interacting anisotropic bodies. For materials like those shown in Figure 4a, the magnitude of $\mathcal{A}^{(2)}$ is much smaller than that of $\mathcal{A}^{(0)}$; thus, $\mathcal{A}^{(2)}$ typically contributes little to the interaction free energy and normal force between bodies. In cases where the interactions have no angular dependence, such as two isotropic, semi-infinite planar bodies acting across an isotropic gap, $\mathcal{A}^{(2)} = 0$. In Figure 4a, interacting planes of anisotropic material (solid lines for all systems) show a nonmonotonic variation of $\mathcal{A}^{(2)}$ with separation. This nonmonotonic variation of the Hamaker coefficient, sometimes leading also to nonmonotonic dependence of the interaction free energy, has been observed in the case of vdW interactions in the system composed of an ice layer interacting with air across a liquid water layer.[38] In that case, similarly as in our own, the nonmonotonicity results from a subtle interplay of dielectric anisotropy, inhomogeneity, and the finite velocity of light, and is thus a signature of the retardation effects.

For interacting composite planes and for an interacting cylinder pair, Figure 4a shows nonzero values for both the anisotropic material (solid lines) cases as well as the isotropic material (dashed lines) cases. In general, both the highly anisotropic shape of cylinders as well as the anisotropy of the materials' responses contribute to the values of $\mathcal{A}^{(2)}$. However, in the case of interacting planes, only the material anisotropy contributes to $\mathcal{A}^{(2)}$. Figure 4b shows that the contribution of $\mathcal{A}^{(2)}$ relative to the total Hamaker coefficients, $\mathcal{A}^{(2)}/(\mathcal{A}^{(0)} + \mathcal{A}^{(2)})$, is greatly increased by the inclusions of morphological anisotropy in the composite and pair cases when compared to the planar cases (green and magenta curves) which contain no morphological anisotropy. A detailed view in the inset shows that, for composites and cylinder pairs, even


DOI: 10.1021/acs.jpcc.5b01870
J. Phys. Chem. C 2015, 119, 19083−19094

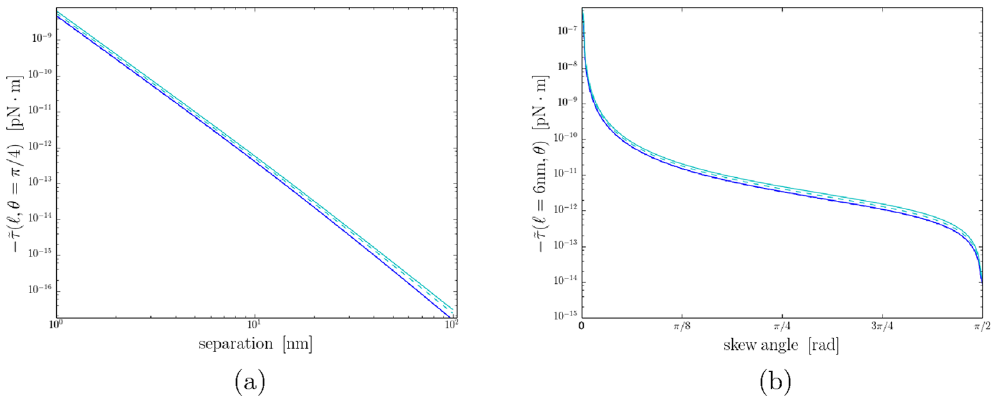


**Figure 7.** (a) Torque per isolated pair of cylinders, $\tilde{\tau}$, at a mutual angle of $\theta = \pi/4$ plotted as a function of separation for cylinders of anisotropic (solid lines) or isotropic (dashed lines) [6,5,s] (blue) or [9,3,m] (cyan) material. (b) Torque as a function of mutual angle, $\theta$, between a pair of cylinders interacting across a 6 nm gap. Cylinders made of either anisotropic or isotropic material will experience torques that drive them to seek parallel alignment of their longitudinal axes.

isotropic materials (dashed lines) have large values of $\mathcal{A}^{(2)}$ which are comparable in magnitude to their analogous cases with anisotropic materials (solid lines).

**Effects on van der Waals Interaction Free Energy.** The free energies of interaction, $\mathcal{G}(l, \theta)$, for planar and composite cases are calculated per unit area, $S$. Figure 5a shows similar behavior for the free energies per 1 nm$^2$ as a function of separation for planes and composites for the cases of anisotropic materials (solid lines) and isotropic materials (dashed lines). However, Figure 5a (inset) shows that free energies of composites have a much stronger dependence on mutual angle than planar cases. The values of interaction free energies given for two interacting cylinders as a function of separation in Figure 5b show a behavior similar to that seen for planes and composites. The free energy expression for a pair of cylinders carries an additional $\theta$ dependence of $\sin^{-1}\theta$ with both Hamaker coefficients, eq 20, that is not present in the expressions for planar and composite cases. Therefore, Figure 5b (inset) shows a stronger dependence of the free energy between two cylinders on mutual angle than seen in Figure 5a (inset) for planes and composites.

**Effects on van der Waals Torque.** The interaction free energy per unit area for planes and composites are differentiated with respect to mutual angle and plotted as torque per 1 nm$^2$ area at $\pi/4$ radians as a function of separation for bodies made of anisotropic materials (solid lines) and isotopic materials (dashed lines) in Figure 6a. Though the values of free energy are similar for interacting planes and composites at maximum packing fraction, see Figure 5a, their torque values are dissimilar at all volume fractions, evidencing the effect of morphological anisotropy introduced by the inclusion of cylinders in composite bodies. Significantly, though the composite case with, e.g., maximum volume fraction (red and black curves), has less interacting material than the planar case (green and magenta curves) it shows much larger values of torque for both cases of anisotropic material and isotropic material in Figure 6.

In Figure 7a, the torque experienced between a pair of interacting cylinders inclined at $\pi/4$ radians is plotted as a function of separation. Torque values show similar dependence on separation compared to those of planes and composites, but of course, lower magnitude due to the reduced dimensionality of the calculation. Comparable magnitudes would be obtained if one would multiply the torque of a lone pair of cylinders by the appropriate surface density in a composite body. The free energy of interaction for a pair of cylinders has two angle-dependent factors and consequently a stronger dependence of torque on mutual angle, shown at a separation of 6 nm in Figure 7b.

## ■ CONCLUSIONS

The effects of anisotropy on vdW interactions are complicated and can be traced to two or fewer properties of a system. Angular dependence of the vdW interaction between bodies can originate from either the anisotropy of the shape of the bodies (morphological anisotropy) or anisotropy of dielectric response of the materials (materials anisotropy) of the bodies. Each system can have one, both, or neither of these properties which allow angular dependencies in the interaction free energy.

**Isolation of Material-Anisotropy Effects.** The case of two interacting anisotropic semi-infinite planar slabs shows angular dependence of the interactions purely due to the anisotropic material response. When the interfaces are made of isotropic material, the free energy loses all dependence on orientation, the angular dependent term, $\mathcal{A}^{(2)}$ drops out of the free energy, and consequently the system displays no torque between the apposed planar interfaces. Two interacting anisotropic semi-infinite planar interfaces are a prime example of anisotropic vdW interactions originating solely in the material dielectric response anisotropy of the bodies.

**Isolation of Shape-Anisotropy Effects.** For an isolated pair of cylinders, the vdW interaction free energy depends on interaxial separation, and its dependence on mutual orientation angle contains both shape anisotropy and material anisotropy effects. Unlike anisotropic planes, which carry angular dependence of $\cos 2\theta$ with only the $\mathcal{A}^{(2)}$ term in the Hamaker coefficient, cylinders carry an additional $\sin^{-1}\theta$ dependence on mutual angle with both Hamaker coefficients, see eq 20, because of their anisotropic shape. Two interacting cylinders composed of isotropic material are a prime example of anisotropic vdW interactions originating solely in the shape anisotropy of the bodies.

**Effects in Composite Bodies.** The formulas for interacting composite bodies exhibit both types of anisotropy effects as a natural consequence of the process of embedding arrays of anisotropic cylinders into two half-spaces with planar interfaces.


DOI: 10.1021/acs.jpcc.5b01870
J. Phys. Chem. C 2015, 119, 19083−19094

The anisotropic shape of the long, thin, embedded cylinders in addition to the anisotropic response of the material from which the cylinders are made result in strong angular dependence and large vdW torques generated between the bodies. Even in cases where the material of the cylinders in the arrays have isotropic dielectric responses, we still see large torque values due to the shape of cylinders. Arrays of cylinders will therefore seek to align their principal dielectric axes even if the material is isotropic.

Torque values between composite bodies larger than those between planes are a corollary to the process of embedding cylinder arrays into planes. Unlike the small change effected by this process on the free energies of these two systems, the effect on torque is dramatic. This effect of anisotropy in a composite material can be seen in the increase in the orientational Hamaker coefficient, $\mathcal{A}^{(2)}$, see Figure 4. The magnitude of $\mathcal{A}^{(2)}$ is carried through the differentiation of free energy with respect to the mutual angle, i.e., torque, between the bodies and results in values much larger than those of solid bodies. The increase in anisotropy and torque is largest for close packing and is drastically reduced as the arrays become dilute. The effect of shape in interactions between composite bodies comprising arrays of parallel cylinders results in torques significantly stronger than those seen between solid anisotropic planar spaces. This clearly points to the nonadditivity of the shape and material anisotropies in this case, which is an important conclusion to bear in mind when trying to detect the vdW torques between anisotropic bodies. The anisotropic shape of the embedded cylinders in composite bodies increases the anisotropy between the bulk dielectric responses in the parallel and perpendicular directions for the composite body, see Figure 2. The zero-frequency thermal contribution to the free energy, i.e., the $n = 0$ term in the sum over Matsubara frequencies, is the frequency most effected by this change. For example, the zero-frequency term of the perpendicular dielectric response of a [6,5,s] CNT composite increases by 63% and its parallel response is nearly doubled. For the [9,3,m] CNT composite at maximum volume fraction, the zero-frequency term in the perpendicular response increases by 66% while the parallel response decreases by 3%. As the separation between cylinders increases (volume fraction decreases), the zero-frequency term of the dielectric response of the composite begins to approach the zero-frequency term of the dielectric response of water; thus, the dielectric contrast with the intervening medium is decreased.

**Experimental Points.** Though the vdW torque between anisotropic bodies is small,[12,39] it seems to be measurable, with a direct experiment still lacking.[40,41] From the discussion above and from related work by Esquivel-Sirvent and Schatz,[42] it seems that the vdW torques between ordered arrays of anisotropic nanoparticles embedded in an isotropic matrix would be a good direction for experiments. Such arrays are well-known and have been observed with many biological macromolecules including DNA, various polysaccharides such as cellulose or hyaluronic acid, and polypeptides such as microtubules or actin, to name just a few (for details see Yasar et al.[43] and references therein). Cylindrical arrays with hexagonal local symmetry observed in DNA-covered single-walled carbon nanotubes (SWCNTs)[44] or surfactant-covered SWCNTs[45] fall well within the confines of our theoretical model of anisotropic arrays. Another possibility that we do not consider here, though it is implied by the (nematic) ordering of the array of cylinders, is the action of external fields on the dielectric properties of interacting bodies.[30] The fact that ordered arrays of cylinders lead to pronounced vdW torques could be exploited in filament-gliding assays above planes composed of layers of locally aligned microtubules with grain boundaries between regions array orientation.[46] The vdW torque could possibly influence the direction of motion of the gliding filament as it crosses the orientational grain boundary.

## SUMMARY

Orientational dependence in the full Lifshitz formulation of van der Waals interactions generally results from two system properties, shown here as (1) anisotropy of materials' bulk dielectric responses in the axial and radial directions and (2) anisotropic morphology demonstrated here by long, thin shape of cylinders in pairs or in arrays embedded in composite planes. The effects of these two properties are isolated through analysis of three interaction geometries: planes, composite planes, and a cylinder pair. Each of the three systems characterizes different strengths of dependencies on the anisotropies of materials' responses and/or bodies' shapes. Interacting composite bodies made of arrays of parallel cylinders embedded in a medium display dependence on both material and shape anisotropies, resulting in values of torque between the arrays that, surprisingly, can be stronger than those between planes and may lead to new experimental possibilities.

## APPENDIX A: DERIVATION OF THE FREE ENERGY OF INTERACTION FOR TWO SEMI-INFINITE ANISOTROPIC UNIAXIAL PLANES

The full Lifshitz free energy of interaction per unit area for two uniaxial anisotropic half spaces, "1" and "2", whose principal dielectric axes are inclined at a fixed angle, interacting across an isotropic medium, $\mathcal{G}(l, \theta)$, is given as a function of separation, $l$, and mutual orientation angle, $\theta$, in the form first derived by Barash:[8,9]

$$\mathcal{G}(l, \theta) = -\frac{\mathcal{H}(l, \theta)}{12\pi l^2} \tag{23}$$

where we have explicitly isolated the $l^{-2}$ dependence from

$$\mathcal{G}(l, \theta) = \frac{3k_{\mathrm{B}}T}{2}\sum_{n=0}^{\infty}{}' \int_0^{\infty} Q\, \mathrm{d}Q \int_0^{2\pi} \mathrm{d}\phi \log \mathcal{D}(l, \theta; Q, \phi) \tag{24}$$

to be able to introduce the standard form of the Hamaker coefficient as in eq 23. $\mathcal{D}(l, \theta; Q, \phi)$ is the *secular determinant* of all allowed surface modes with magnitude of the in-plane wave-vector, $Q$, of the fluctuating electromagnetic field that depends on $l$ and $\theta$. The summation over the Matsubara frequencies, $\omega_n = 2\pi n k_{\mathrm{B}}T/\hbar$ with the $n = 0$ term weighted by one-half, stems from the thermal bath of the fluctuating field. At room temperature, the Matsubara frequencies are multiples of $2.4 \times 10^{14}\ \mathrm{s}^{-1}$.

The secular determinant, $\mathcal{D}(l,\theta; Q, \phi)$, depends also on two additional parameters (the magnitude $Q$ and the direction $\phi$ of the in-plane wave vector, which are both integrated over) and is given explicitly as

$$\mathcal{D} = [A - \epsilon_{2\perp}(\tilde{\rho}_2 - \rho_2)(B - E + C)]/\gamma \tag{25}$$


DOI: 10.1021/acs.jpcc.5b01870
J. Phys. Chem. C 2015, 119, 19083−19094

where

$$\gamma = (\rho_1 + \rho_3)(\rho_2 + \rho_3)((\epsilon_3\rho_1 + \epsilon_{1\perp}\rho_3)(\rho_1{}^2 - Q^2\sin^2\phi) - (\epsilon_{1\perp}(\tilde{\rho}_1 - \rho_1)(Q^2\sin^2\phi - \rho_1\rho_3)))((\epsilon_3\rho_2 + \epsilon_{2\perp}\rho_3)(\rho_2{}^2 - Q^2(\cos\phi\sin\theta + \sin\phi\cos\theta)(\cos\phi\sin\theta + \sin\phi\cos\theta)) - (\epsilon_{2\perp}(\tilde{\rho}_2 - \rho_2)(Q^2(\cos\phi\sin\theta + \sin\phi\cos\theta)(\cos\phi\sin\theta + \sin\phi\cos\theta) - \rho_2\rho_3))) \quad (26)$$

and

$$A = ((\rho_1 + \rho_3)(\rho_2 + \rho_3) - (\rho_1 - \rho_3)(\rho_2 - \rho_3)e^{-2\rho_3})((\epsilon_3\rho_1 + \epsilon_{1\perp}\rho_3)(\epsilon_3\rho_2 + \epsilon_{2\perp}\rho_3) - (\epsilon_3\rho_1 - \epsilon_{1\perp}\rho_3)(\epsilon_3\rho_2 - \epsilon_{2\perp}\rho_3)e^{-2\rho_3})(\rho_1{}^2 - Q^2\sin^2\phi)(\rho_2{}^2 - Q^2\sin(\phi + \theta)\sin(\phi + \theta))((\epsilon_{1\perp}(\tilde{\rho}_1 - \rho_1)))((Q^2\sin^2\phi - \rho_1\rho_3)(\epsilon_3\rho_2 + \epsilon_{2\perp}\rho_3)(\rho_2 + \rho_3)(\rho_1 + \rho_3) + 2(\epsilon_{2\perp} - \epsilon_3) - (Q^2\sin^2\phi(Q^2\rho_1 - \rho_2\rho_3{}^2) + \rho_1\rho_3{}^2(Q^2 - 2Q^2\sin^2\phi + \rho_1\rho_2))e^{-2\rho_3} + (Q^2\sin^2\phi + \rho_1\rho_3)(\epsilon_3\rho_2 - \epsilon_{2\perp}\rho_3)(\rho_1 - \rho_3)(\rho_2 - \rho_3)e^{-4\rho_3}) \quad (27)$$

and

$$B = ((\epsilon_3\rho_1 + \epsilon_{1\perp}\rho_3)(\rho_1 + \rho_3)(\rho_2 + \rho_3) + 2(\epsilon_{1\perp} - \epsilon_3)(Q^2\rho_2 - \rho_1\rho_3{}^2 - 2\rho_2\rho_3{}^2)e^{-2\rho_3} + (\epsilon_3\rho_1 - \epsilon_{1\perp}\rho_3)(\rho_1 - \rho_3)(\rho_2 - \rho_3)e^{-4\rho_3})(\rho_1{}^2 - Q^2\sin^2\phi) + (\epsilon_{1\perp}(\tilde{\rho}_1 - \rho_1))(-(Q^2\sin^2\phi - \rho_1\rho_3)(\rho_1 + \rho_3)(\rho_2 + \rho_3) + 2(Q^2\sin^2\phi(\rho_1\rho_2 + \rho_3{}^2) - \rho_1{}^2\rho_3{}^2 + \rho_1\rho_2\rho_3{}^2)e^{-2\rho_3} - (Q^2\sin^2\phi + \rho_1\rho_3)(\rho_1 - \rho_3)(\rho_2 - \rho_3)e^{-4\rho_3})Q^2\sin(\phi + \theta)\sin(\phi + \theta) \quad (28)$$

and

$$C = \rho_2\rho_3(-(\epsilon_3\rho_1 + \epsilon_{1\perp}\rho_3)(\rho_1 + \rho_3)(\rho_2 + \rho_3) + 2\rho_3(\epsilon_{1\perp} - \epsilon_3)(r2 + \rho_1\rho_2)e^{-2\rho_3} + (\epsilon_3\rho_1 - \epsilon_{1\perp}\rho_3)(\rho_1 - \rho_3)(\rho_2 - \rho_3)e^{-4\rho_3})(\rho_1{}^2 - Q^2\sin^2\phi) + \epsilon_{1\perp}(\tilde{\rho}_1 - \rho_1)\rho_2\rho_3((Q^2\sin^2\phi - \rho_1\rho_3)(\rho_1 + \rho_3)(\rho_2 + \rho_3) + 2\rho_3(\rho_1{}^2\rho_2 + \rho_1\rho_3{}^2 + Q^2\sin^2\phi(\rho_1 - \rho_2))e^{-2\rho_3} - (Q^2\sin^2\phi + \rho_1\rho_3)(\rho_1 - \rho_3)(\rho_2 - \rho_3)e^{-4\rho_3}) \quad (29)$$

and

$$E = 4\rho_1\rho_2\rho_3{}^2\epsilon_{1\perp}(\tilde{\rho}_1 - \rho_1)e^{-2\rho_3}(2Q^2\sin\phi\cos\theta\sin(\phi + \theta) + \rho_3{}^2\sin\theta\sin\theta) \quad (30)$$

The dimensionless wave vectors for plane 1, plane 2, and medium 3 are given as

$$\rho_1{}^2 = Q^2 + \epsilon_{1\perp}\frac{\xi^2 l^2}{c^2},\ \rho_2{}^2 = Q^2 + \epsilon_{2\perp}\frac{\xi^2 l^2}{c^2},\ \rho_3{}^2 = Q^2 + \epsilon_3\frac{\xi^2 l^2}{c^2}$$
$$\tilde{\rho}_1{}^2 = Q^2 + (\epsilon_{1\parallel}/\epsilon_{1\perp} - 1)Q^2\cos^2\phi + \epsilon_{1\parallel}\frac{\xi^2 l^2}{c^2}$$
$$\tilde{\rho}_2{}^2 = Q^2 + (\epsilon_{2\parallel}/\epsilon_{2\perp} - 1)r^2(\cos\phi\cos\theta - \sin\phi\sin\theta)^2 + \epsilon_{2\parallel}\frac{\xi^2 l^2}{c^2} \quad (31)$$

There appears to be no known simplification of this result. A different form of the interaction free energy was derived in ref 15 that numerically reduces to the result above, but it was not shown to reduce to it exactly and/or analytically. In the main text, we used the above derivation in the symmetric case of “1” = “2”.

## ■ APPENDIX B: DERIVATION OF THE FREE ENERGY OF INTERACTION FOR TWO CYLINDERS

By beginning with the expressions for two composite planar media, “1” and “2”, at a separation $l$, made of arrays of parallel cylinders embedded in isotropic medium, the free energy of an isolated pair of inclined cylinders is derived by taking the volume fraction of the composite in the dilute limit and expanding the anisotropic dielectric responses to second order in the number density.[2] The exact relation is

$$\frac{d^2\mathcal{G}(l, \theta)}{dl^2} = N_1N_2\sin\theta\, G(l, \theta) \quad (32)$$

where the area density of the cylinders $(N_1, N_2)$ in the direction of their long axes is $\nu_1 = N_1\pi\alpha_1{}^2$ $(\nu_2 = N_2\pi\alpha_2{}^2)$ and the interaction free energy between the two cylinders whose axes are contained within the two parallel boundaries at a separation $l$, but skewed at an angle $\theta$ is $G(l, \theta)$. The second derivative can be written furthermore as

$$\frac{d^2\mathcal{G}(l, \theta)}{dl^2} = \frac{k_BT}{2\pi}\sum_{n=0}^{\infty}{}' \int_0^\infty Q\, dQ \frac{d^2 f(Q, \omega_n; l, \theta)}{dl^2} \quad (33)$$

where

$$\frac{d^2 f(Q, \omega_n; l, \theta)}{dl^2} = -\frac{\nu_1\nu_2\Delta_{1,\parallel}\Delta_{2,\parallel}}{32}\frac{\exp\left(-2l\sqrt{Q^2 + \epsilon_m\frac{\omega_n^2}{c^2}}\right)}{\left(Q^2 + \epsilon_m\frac{\omega_n^2}{c^2}\right)}\left\{2[(1 + 3a_1)(1 + 3a_2)Q^4 + 2(1 + 2a_1 + 2a_2 + 3a_1a_2)Q^2\epsilon_m\frac{\omega_n^2}{c^2} + 2(1 + a_1)(1 + a_2)\epsilon_m^2\frac{\omega_n^4}{c^4}] + (1 - a_1)(1 - a_2)\left(Q^2 + 2\epsilon_m\frac{\omega_n^2}{c^2}\right)^2\cos 2\theta\right\} \quad (34)$$

and the relative anisotropy measures are

$$a = \frac{2\Delta_\perp}{\Delta_\parallel} = 2\frac{(\epsilon_\perp^c - \epsilon_m)\epsilon_m}{(\epsilon_\perp^c + \epsilon_m)(\epsilon_\parallel^c - \epsilon_m)} \quad (35)$$

for the two composite materials 1 and 2.

The vdW interaction free energy between the two inclined cylinders of radii $R_1$ and $R_2$ composed of anisotropic material is given as


DOI: 10.1021/acs.jpcc.5b01870
J. Phys. Chem. C 2015, 119, 19083−19094

$$G(l, \theta) = -\frac{(\pi R_1^2)(\pi R_2^2)}{2\pi l^4 \sin\theta}(\mathcal{A}^{(0)}(l) + \mathcal{A}^{(2)}(l)\cos 2\theta) \quad (36)$$

Where the Hamaker coefficients are

$$\mathcal{A}^{(0)}(l) = \frac{k_B T}{32}\sum_{n=0}^{\infty}{}' \Delta_{1,\|}\Delta_{2,\|}p_n^{\ 4}(l) \int_0^\infty t\ \mathrm{d}t \frac{\exp\left(-2p_n(l)\sqrt{t^2+1}\right)}{(t^2+1)}\tilde{g}^{(0)}(t, a_1(\mathrm{i}\omega_n), a_2(\mathrm{i}\omega_n))$$

with

$$\tilde{g}^{(0)}(t, a_1(\mathrm{i}\omega_n), a_2(\mathrm{i}\omega_n)) = [(1+3a_1)(1+3a_2)t^4 + 2(1+2a_1+2a_2+3a_1a_2)t^2 + 2(1+a_1)(1+a_2)] \quad (37)$$

and

$$\mathcal{A}^{(2)}(l) = \frac{k_B T}{32}\sum_{n=0}^{\infty}{}' \Delta_{1,\|}\Delta_{2,\|}p_n^{\ 4}(l) \int_0^\infty t\ \mathrm{d}t \frac{\exp\left(-2p_n(l)\sqrt{t^2+1}\right)}{(t^2+1)}\tilde{g}^{(2)} (t, a_1(\mathrm{i}\omega_n), a_2(\mathrm{i}\omega_n)\theta)$$

with

$$\tilde{g}^{(2)}(t, a_1(\mathrm{i}\omega_n), a_2(\mathrm{i}\omega_n)\theta) = (1-a_1)(1-a_2)(t^2+2)^2 \quad (38)$$

with

$$u = Ql, \ \ p_n^{\ 2}(l) = \epsilon_m(\mathrm{i}\omega_n)\frac{\omega_n^{\ 2}}{c^2}l^2; \ \text{thus, } u = p_n t \quad (39)$$

From the form of eq 36 for the interaction free energy, it is clear that the free energy of a pair of identical cylinders because of the factor $\sin^{-1}\theta$ thus carries angular dependence with both Hamaker coefficients, $\mathcal{A}^{(0)}$ and $\mathcal{A}^{(2)}$, unlike the planar and composite cases which have explicit angular dependence only in the orientation term, $\mathcal{A}^{(2)}$. In the main text we used the above derivation in the symmetric case of "1" = "2" with $R_1 = R_2 = \alpha$.

## AUTHOR INFORMATION


### Corresponding Author

*E-mail: podgornik@physics.umass.edu.


### Notes

The authors declare no competing financial interest.

## ACKNOWLEDGMENTS


This research was supported by the US Department of Energy, Office of Basic Energy Sciences, Division of Materials Sciences and Engineering under Awards DE-SC0008176 and DE-SC0008068. W.Y.C. expresses appreciation for the resources provided by the National Energy Research Scientific Computing Center supported by DOE under Contract DE-AC03-76SF00098. R.P. thanks Raul Esquivel-Sirvent for his comments on an earlier version of the manuscript.


## REFERENCES


(1) Schematics by Hopkins, J. C.; rendered in part using TubeGen 3.4. http://turin.nss.udel.edu/research/tubegenonline.html (accessed November 14, 2014) and PyMOL Molecular Graphics System Version 1.7.1.3. www.pymol.org (accessed November 14, 2014) .

(2) Parsegian, V. A. *van der Waals Forces*; Cambridge University Press: Cambridge, U.K., 2005.

(3) French, R.; et al. Long range interactions in nanoscale science. *Rev. Mod. Phys.* **2010**, *82*, 1887−1944.

(4) Dryden, D. M.; Hopkins, J. C.; Denoyer, L. K.; Poudel, L.; Steinmetz, N. F.; Ching, W. Y.; Podgornik, R.; Parsegian, V. A.; French, R. H. van der Waals Interactions at the Mesoscale: Open-Science Implementation, Anisotropy, Retardation, and Solvent Effects. *Langmuir* **2015**, DOI: 10.1021/acs.langmuir.5b00106.

(5) Kats, E. I. On the optical activity in mixtures of liquid crystals. *Sov. Phys. JETP* **1978**, *13* (47), 1205−1210.

(6) Kornilovitch, P. E. van der Waals interaction in uniaxial anisotropic media. *J. Phys.: Condens. Matter* **2013**, *25*, 035102.

(7) Parsegian, V. A.; Weiss, G. H. Dielectric anisotropy and the van der Waals interaction between bulk media. *J. Adhes.* **1972**, *3*, 259.

(8) Barash, Yu. S. Moment of van der Waals forces between anisotropic bodies. *Radiophys. Quantum Electron.* **1978**, *21*, 1138−1143.

(9) Barash, Yu. S. van der Waals interaction between anisotropic bodies. *Radiophys. Quantum Electron.* **1973**, *16*, 945−949.

(10) van Enk, S. J. Casimir torque between dielectrics. *Phys. Rev. A: At., Mol., Opt. Phys.* **1995**, *52*, 2569−2575.

(11) Shao, C. G.; Tong, A. H.; Luo, J. Casimir torque between two birefringent plates. *Phys. Rev. A: At., Mol., Opt. Phys.* **2005**, *72*, 022102.

(12) Munday, J. N.; Iannuzzi, D.; Barash, Yu. S.; Capasso, F. Torque on birefringent plates induced by quantum fluctuations. *Phys. Rev. A: At., Mol., Opt. Phys.* **2005**, *71*, 042102.

(13) Munday, J. N.; Iannuzzi, D.; Barash, Yu. S.; Capasso, F. Erratum: Torque on birefrigent plates induced by quantum fluctuations. *Phys. Rev. A: At., Mol., Opt. Phys.* **2008**, *78*, 029906.

(14) Veble, G.; Podgornik, R. Dispersion interactions in stratified anisotropic and optically active media at all separations. *Phys. Rev. B: Condens. Matter Mater. Phys.* **2009**, *80*, 075422.

(15) Philbin, T. G.; Leonhardt, L. An alternative calculation of the Casimir forces between birefringent plates. *Phys. Rev. A: At., Mol., Opt. Phys.* **2008**, *78*, 042107.

(16) Veble, G.; Podgornik, R. The boundary element approach to van der Waals interactions. *Eur. Phys. J. E: Soft Matter Biol. Phys.* **2007**, *23*, 275−279.

(17) Emig, T.; Graham, N.; Jaffe, R. L.; Kardar, M. Orientation dependence of Casimir forces. *Phys. Rev. A: At., Mol., Opt. Phys.* **2009**, *79*, 054901.

(18) Rahi, S. J.; Emig, T.; Jaffe, R. L. Geometry and material effects in Casimir physics-scattering theory. *Casimir Physics, Lecture Notes in Physics* **2011**, *21* (834), 129−174.

(19) Banishev, A. A.; Wagner, J.; Emig, T.; Zandi, R.; Mohideen, U. Demonstration of angle-dependent Casimir force between corrugations. *Phys. Rev. Lett.* **2013**, *110*, 250403.

(20) Banishev, A. A.; Wagner, J.; Emig, T.; Zandi, R.; Mohideen, U. Experimental and theoretical investigation of the angular dependence of the Casimir force between sinusoidally corrugated surfaces. *Phys. Rev. B: Condens. Matter Mater. Phys.* **2014**, *89*, 235436.

(21) Pitaevskii, L. P. Thermal Lifshitz force between an atom and a conductor with a small density of carriers. *Phys. Rev. Lett.* **2008**, *101* (16), 163202.

(22) Barash, Yu. S.; Kyasov, A. A. Interaction potential for two filaments and for an atom interacting with a filament. *Sov. Phys. JETP* **1989**, *68*, 39.

(23) Rajter, R. F.; Podgornik, R.; Parsegian, V. A.; French, R. H.; Ching, W. Y. van der Waals-London dispersion interactions for optically anisotropic cylinders: Metallic and semiconducting single-wall carbon nanotubes. *Phys. Rev. B: Condens. Matter Mater. Phys.* **2007**, *76*, 045417.




DOI: 10.1021/acs.jpcc.5b01870
J. Phys. Chem. C 2015, 119, 19083−19094

(24) Siber, A.; Rajter, R. F.; French, R. H.; Ching, W. Y.; Parsegian, V. A.; Podgornik, R. Dispersion interactions between optically anisotropic cylinders at all separations: Retardation effects for insulating and semiconducting single-wall carbon nanotubes. *Phys. Rev. B: Condens. Matter Mater. Phys.* **2009**, *80*, 165414.
(25) Siber, A.; Rajter, R. F.; French, R. H.; Ching, W. Y.; Parsegian, V. A.; Podgornik, R. Optically anisotropic infinite cylinder above an optically anisotropic half-space: Dispersion interaction of a single-walled carbon nanotube with a substrate. *J. Vac. Sci. Technol. B* **2010**, *28*, C4A17.
(26) Saville, D. A.; Chun, J.; Li, J. L.; Schniepp, H. C.; Car, R.; Aksay, I. A. Orientational order of molecular assemblies on inorganic crystals. *Phys. Rev. Lett.* **2006**, *96*, 018301.
(27) Noruzifar, E.; Emig, T.; Zandi, R. Universality versus material dependence of fluctuation forces between metallic wires. *Phys. Rev. A: At., Mol., Opt. Phys.* **2011**, *84*, 042501.
(28) Rodriguez-Lopez, P.; Emig, T. Casimir interaction between inclined metallic cylinders. *Phys. Rev. A: At., Mol., Opt. Phys.* **2012**, *85*, 032510.
(29) Emig, T. Casimir physics: Geometry, shape and material. *Int. J. Mod. Phys. A* **2010**, *25*, 2177−2195.
(30) Esquivel-Sirvent, R.; Cocoletzi, G. H.; Palomino-Ovando, M. van der Waals torque induced by external magnetic fields. *J. Appl. Phys.* **2010**, *108*, 114101.
(31) Mahanty, J.; Ninham, B. W. *Dispersion Forces*; Academic Press: New York, 1976.
(32) Rajter, R. F.; French, R. H.; Podgornik, R.; Ching, W. Y.; Parsegian, V. A. Spectral mixing formulations for van der Waals-London dispersion interactions between multicomponent carbon nanotubes. *J. Appl. Phys.* **2008**, *104*, 053513.
(33) Esquivel-Sirvent, R.; Schatz, G. C. Mixing rules and the Casimir force between composite systems. *Phys. Rev. A: At., Mol., Opt. Phys.* **2011**, *83*, 042512.
(34) Maron, N.; Maron, O. On the mixing rules for astrophysical inhomogeneous grains. *Mon. Not. R. Astron. Soc.* **2005**, *357*, 873.
(35) Gecko Hamaker:An Open-Science Software Tool. geckoproj.sourceforge.net (accessed May 20, 2015) .
(36) Ching, W. Y.; Rulis, P. *Electronic Structure Methods for Complex Materials: The Orthogonalized Linear Combination of Atomic Orbitals*. Oxford University Press: Oxfor, U.K., 2012.
(37) Rajter, R. F.; French, R. H.; Ching, W. Y.; Podgornik, R.; Parsegian, V. A. Chirality-dependent properties of carbon nanotubes: electronic structure, optical dispersion properties, Hamaker coefficients and van der Waals-London dispersion interactions. *RSC Adv.* **2013**, *3*, 823−842.
(38) Elbaum, M.; Schick, M. Application of the Theory of Dispersion Forces to the Surface Melting of Ice. *Phys. Rev. Lett.* **1991**, *66*, 1713−1716.
(39) Chen, X.; Spence, J. C. H. On the measurement of the Casimir torque. *Phys. Status Solidi B* **2011**, *248*, 2064−2071.
(40) Iannuzzi, D.; Lisanti, M.; Munday, J. N.; Capasso, F. The design of long range quantum electrodynamical forces and torques between macroscopic bodies. *Solid State Commun.* **2005**, *135*, 618−626.
(41) Capasso, F.; Munday, J. N.; Iannuzzi, D.; Chan, H. B. Casimir forces and quantum electrodynamical torques: Physics and nanomechanics. *IEEE J. Sel. Top. Quantum Electron.* **2007**, *13*, 400−414.
(42) Esquivel-Sirvent, R.; Schatz, G. C. van der Waals torque coupling between slabs composed of planar arrays of nanoparticles. *J. Phys. Chem. C* **2013**, *117*, 5492−5496.
(43) Yasar, S.; Podgornik, R.; Valle-Orero, J.; Johnson, M. R.; Parsegian, V. A. Continuity of states between the cholesteric → line hexatic transition and the condensation transition in DNA solutions. *Sci. Rep.* **2014**, *4*, 6877.
(44) Qiu, X.; Khripin, C. Y.; Ke, F.; Howell, S. C.; Zheng, M. Electrostatically Driven Interactions between Hybrid DNA-Carbon Nanotubes. *Phys. Rev. Lett.* **2013**, *111*, 048301.
(45) Do, C.; Jang, H. S.; Choi, S. M. Hydration forces between surfaces of surfactant coated single-walled carbon nanotubes. *J. Chem. Phys.* **2013**, *138*, 114701.
(46) Liu, L.; Tuzel, E.; Ross, J. L. Loop formation of microtubules during gliding at high density. *J. Phys.: Condens. Matter* **2011**, *23*, 374104.


DOI: 10.1021/acs.jpcc.5b01870
*J. Phys. Chem. C* 2015, 119, 19083−19094